

Evolution, Structure, and Cloud Microphysics of East Asian Monsoon Convection— A Dual-Doppler/Polarimetric Radar Study

Jian-Jian Wang

Mesoscale Atmospheric Processes Branch, NASA Goddard Space Flight Center, and
Goddard Center for Earth Science and Technology, University of Maryland, Baltimore County

Abstract

A primary goal of the South China Sea Monsoon Experiment (SCSMEX, 1998), a major field campaign of the Tropical Rainfall Measuring Mission (TRMM), is to define the development and structure of precipitation systems associated with the South China Sea (SCS) summer monsoon. In this study, dual-Doppler and dual polarimetric radar analysis techniques are used to investigate the evolution, structure, dynamics, and microphysical processes of two mesoscale convective systems observed during the SCS monsoon onset in May 1998.

The precipitation and kinematic structure of mesoscale convection were studied with special attention to significant departures from archetypal tropical oceanic convection. Polarimetric radar inferred microphysical (e.g., hydrometeor type, amount, and size) and rainfall properties are placed in the context of the mesoscale morphology and dual-Doppler derived kinematics for this squall line system. A comparison is made between results from this study for SCSMEX and the previous studies for other tropical regions. We found that precipitation over the SCS monsoon region during the summer monsoon onset was more maritime-like, similar to the precipitation over the Amazon monsoon region during the westerly regime, and very unlike the tropical continental convection in the tropical islands of Maritime Continent and during the easterly regime of the Amazon. Both cases studied here showed lower rain rates and rainwater contents, smaller raindrops, and significantly lower ice water contents between 5 km and 8 km than the precipitation over the other tropical regions with more tropical continental characteristics.

Key word: East Asian monsoon, Doppler/polarimetric radar, mesoscale convection

1. Introduction

The East Asian monsoon is an important component of the regional and global climate. The precipitation processes associated with the summer monsoon play an important role in the agriculture and people's daily life of the Southeast and East Asian countries. For instance, the quasi-stationary rain belt, so called Mei-Yu in China and Baiu in Japan, may cause disastrous floods in the region when excessive rainfall occurs. Although the East Asian summer monsoon attracts more attention when it affects the land area to the north during June-August, the onset of the East Asian summer monsoon starts over the ocean to the south in the SCS region in May (Tao and Chen, 1987).

The structure and evolution of the tropical convection has been studied for decades by many investigators (e.g., Houze 1977, Zipser and LeMone 1980, Jorgensen et al. 1997, Rutledge et al. 1992). However, systematic studies on the mesoscale convection in the summer Asian monsoon region are quite rare prior to the South China Sea Monsoon Experiment (SCSMEX, Lau et al. 2000).

The SCSMEX was an international field experiment conducted in SCS and surrounding areas during May—June 1998. The goal of the mesoscale program was to define the initiation, structure, evolution and dynamics of precipitation processes associated with the SEAM. To accomplish this objective, two Doppler

radars were deployed to form a dual-Doppler radar analysis region (Fig. 1) in the northern SCS. Other conventional meteorological observational platforms including rawinsonde, surface observation network, and rain gauges were also collocated at the radar sites and surrounding areas. These observations allowed for the collection of a comprehensive dataset to describe the environment, evolution, rainfall characteristics, and kinematic structure of the monsoon convective systems.

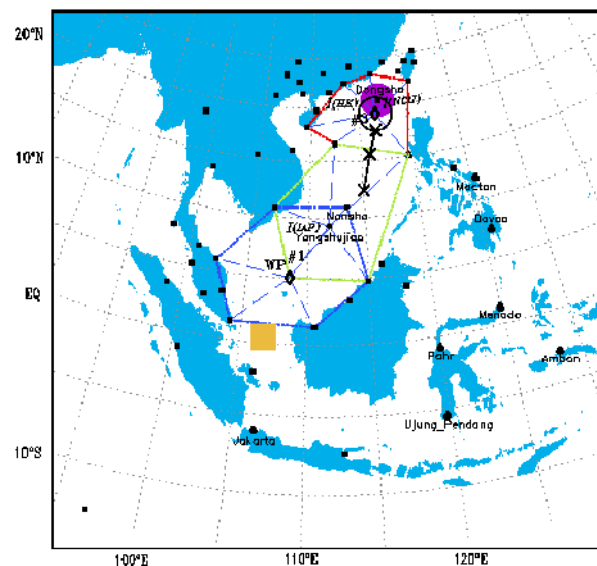


Fig. 1 SCSMEX observing platform.

2. Data analysis

The field phase of SCSMEX was from 1 May to 30 June 1998 including two intensive Observation periods (IOP), 5-25 May and 5-25 June. A variety of instrumentation was deployed in the experiment including C-band Doppler and polarimetric radars forming a dual-Doppler radar network (Fig. 1), enhanced sounding network, and surface meteorological and rainfall observations. The primary data used in this study are radar data including both the conventional and polarimetric variables. The additional sources of information also include synoptic reanalysis charts from National Center for Environmental Prediction (NCEP), Geosynchronous Meteorological Satellite (GMS-5) imagery, sounding network, and automatic weather stations (AWS).

During SCSMEX, the National Oceanographic and Atmospheric Administration (NOAA)/Tropical Oceans Global Atmosphere (TOGA) radar and Bureau of Meteorology Research Centre (BMRC, Australia) polarimetric C-POL radar were deployed to form a dual-Doppler radar network. The C-POL radar was installed at Dongsha Island (20.7°N, 116.7°E) and operated on a 24-h basis (with short breaks) throughout May and June 1998. The TOGA radar was installed on the People's Republic of China *Shiyan* #3 research vessel (about 20.4°N, 116.8°E) and operated continuously during 5-25 May. The length of the radar baseline was about 40-45 km, a frequently used range to provide a good areal coverage with reasonable spatial resolution.

The first step of the radar data analyses in this study is the traditional “dual-Doppler” synthesis methods. Due to a misaligned bandpass filter on the TOGA radar, the reflectivity (Z) measured by the TOGA was significantly biased. Therefore, only the reflectivity data collected from C-POL will be used. Radial velocity data were manually unfolded using the National Center for Atmospheric Research (NCAR) Research Data Support System (RDSS) software. The C-POL radar reflectivity and radial velocity fields were then interpolated to a Cartesian grid using the NCAR REORDER software. Three-dimensional kinematic fields were obtained by using NCAR Custom Editing and Display of Reduced Information in Cartesian space program (CEDRIC, Mohr et al. 1986).

In addition to the dual-Doppler radar analysis, a set of polarimetric variables were also available from C-POL including differential reflectivity (Z_{DR}); total differential phase (Ψ_{DP}); and zero lag correlation coefficient between co-polar horizontal and vertical polarized electro- magnetic waves (ρ_{HV}). These polarimetric variables and specific differential phase (K_{DP}) calculated from Ψ_{DP} can be used to provide information on the size, shape, orientation, and thermodynamic phase of the hydrometers. An analysis of polarimetric radar derived precipitation characteristics, including precipitation ice and liquid water content, was conducted using procedures similar to those outlined in Wang and Carey (2005).

3. Rainfall pattern throughout SCSMEX

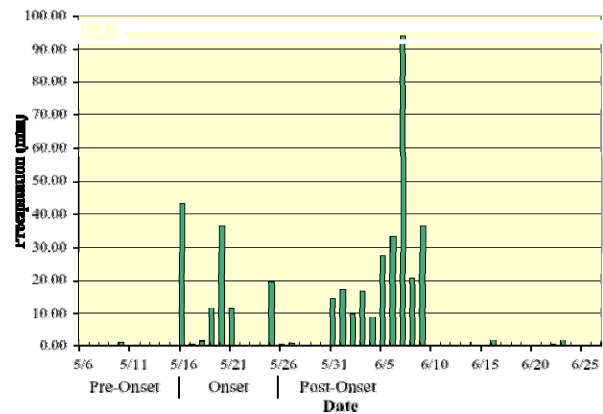


Fig. 2 Daily rainfall recorded at Dongsha Island.

Rainfall recorded at Dongsha Island throughout the SCSMEX (Fig. 2) can be clearly divided into several periods related to the SCS summer monsoon. Prior to 15 May 1998, the SCS region was mainly under the control of the subtropical high over the western Pacific. Although the frontal passages from northwestern China were observed periodically with an interval of 2-4 days, the cloud/rain bands associated with the front weakened and dissipated after moving into the SCS region without any organized precipitation in the area (Figs. 3a and 3b).

In 1998, the SCS summer monsoon onset, starting on May 15, included three steps (Ding and Liu 2001): 1) the low-level southwesterly winds from the tropics prevailed in the northern SCS on 15 May; 2) the southwesterly monsoon flow at low-levels spread to the whole SCS by 20 May; and 3) the upper-level northeasterly winds were established over the SCS region by 23-24 May. On 15 May, a pronounced frontal cloud band oriented from southwest to northeast covered most coastal regions of southeastern China (Fig. 3c). Different from the frontal cloud band reaching the coastal region four days earlier, this system was able to move into the sea without weakening. In fact, after the start of the summer monsoon onset in the northern SCS, the intensity and areal coverage of the frontal cloud bands even became enhanced in the southern portion (partially over the northern SCS) (Fig. 3d). A few days later, influenced by another frontal system spreading from northern SCS to the south of Japan and a tropical cyclone in the Bay of Bengal and Indochina regions that brought more warm and moist air from the tropics, 19-21 May became the rainiest period during the onset stage (Fig. 3d). On 24 May, near the completion of the SCS summer monsoon onset, a mesoscale convective system (MCS) drifting eastward from the southwestern China and northern Indochina peninsula following the prevailing westerly winds associated with a trough to the south of the Tibet Plateau entered the SCS region ((Fig. 3e). A total of three squall lines were observed by the SCSMEX radar network from 2000 LST 24 May to the following day (more details in Section 4).

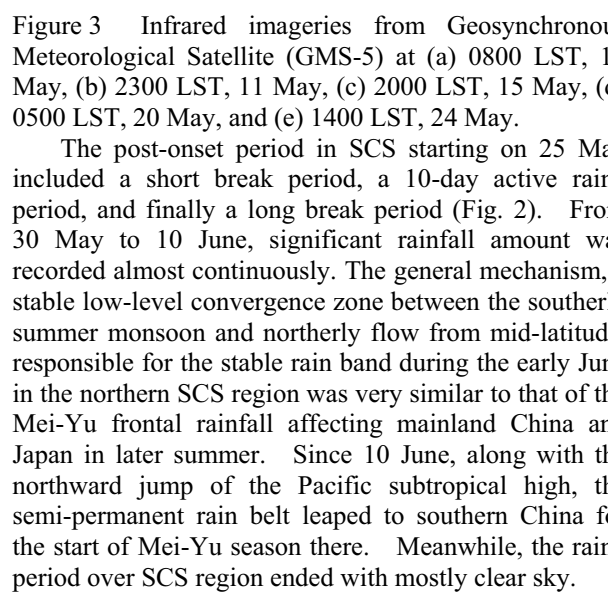
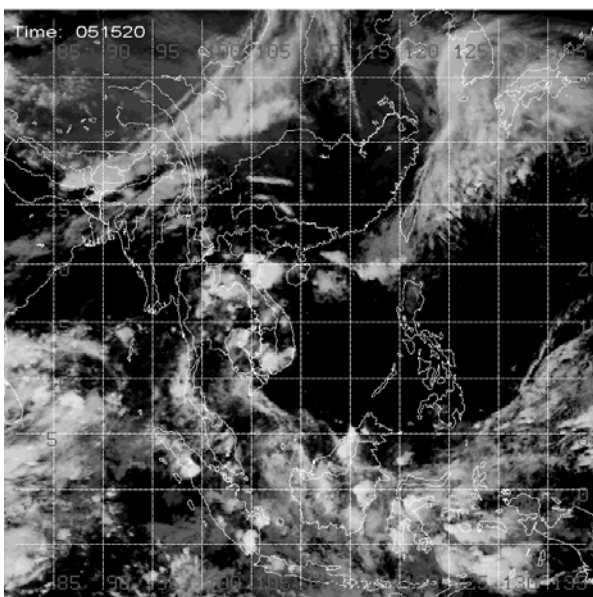
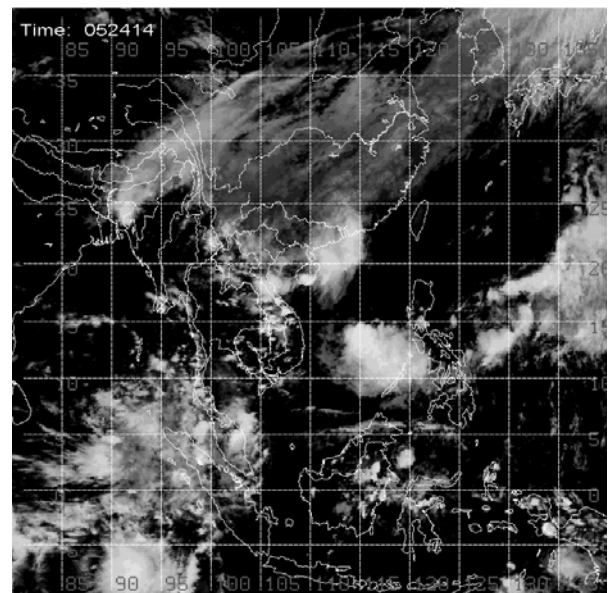
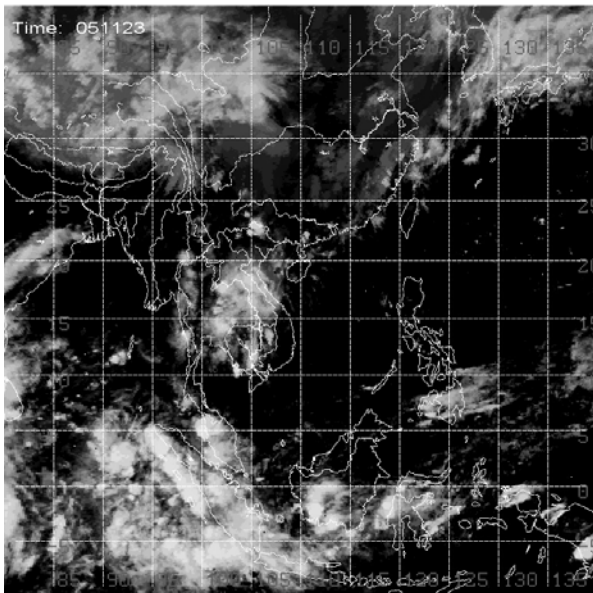
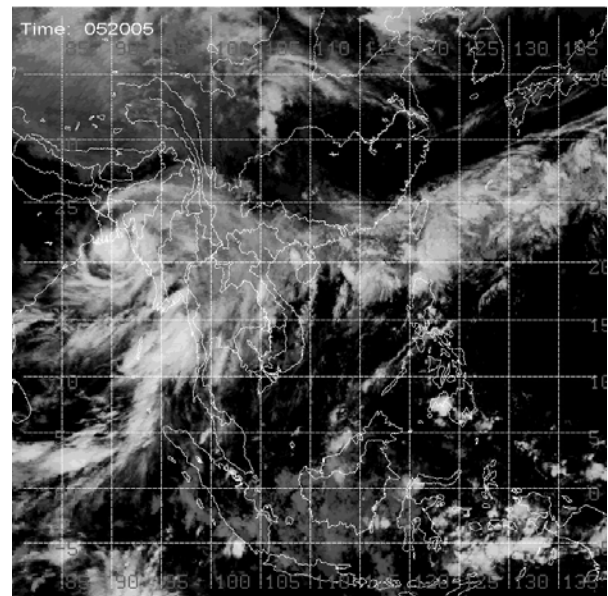
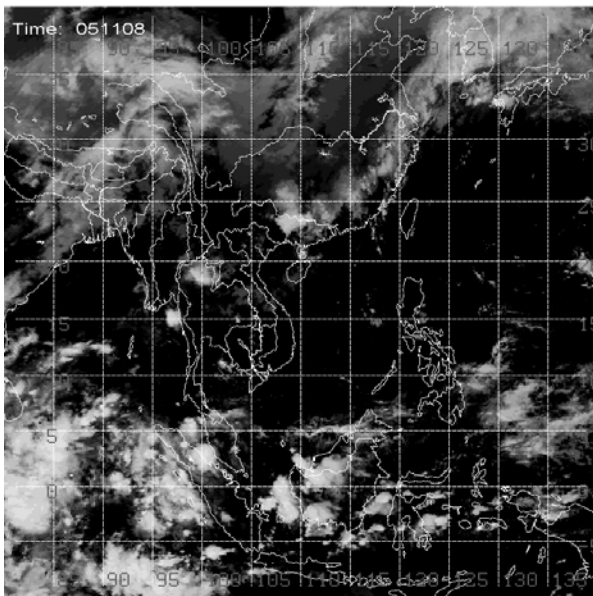


Figure 3 Infrared imageries from Geosynchronous Meteorological Satellite (GMS-5) at (a) 0800 LST, 11 May, (b) 2300 LST, 11 May, (c) 2000 LST, 15 May, (d) 0500 LST, 20 May, and (e) 1400 LST, 24 May.

The post-onset period in SCS starting on 25 May included a short break period, a 10-day active rainy period, and finally a long break period (Fig. 2). From 30 May to 10 June, significant rainfall amount was recorded almost continuously. The general mechanism, a stable low-level convergence zone between the southerly summer monsoon and northerly flow from mid-latitude, responsible for the stable rain band during the early June in the northern SCS region was very similar to that of the Mei-Yu frontal rainfall affecting mainland China and Japan in later summer. Since 10 June, along with the northward jump of the Pacific subtropical high, the semi-permanent rain belt leaped to southern China for the start of Mei-Yu season there. Meanwhile, the rainy period over SCS region ended with mostly clear sky.

4. The evolution, kinematic structure, and microphysics of the convection

There were two types of precipitation processes over the northern SCS during the 10-day monsoon onset period. The first type was the well-organized cloud system related to the frontal systems from northwestern China (Wang 2004, Wang et al. 2007). The interaction between the tropical monsoon flow and the frontal circulation played an important role in the organization and structure of the mesoscale convection. The second type was related to a mesoscale vortex that developed in the northern Indochina peninsula and southern China (Wang and Carey 2005). When a mesoscale vortex drifted eastward along with the southern branch of westerlies around the Tibet Plateau, convection erupted in the northern SCS. The associated rainfall was relatively localized but intense. Waterspouts and squall lines were observed in the northern SCS when influenced by the tropical mesoscale vortex from the west.

a. Case of 20 May

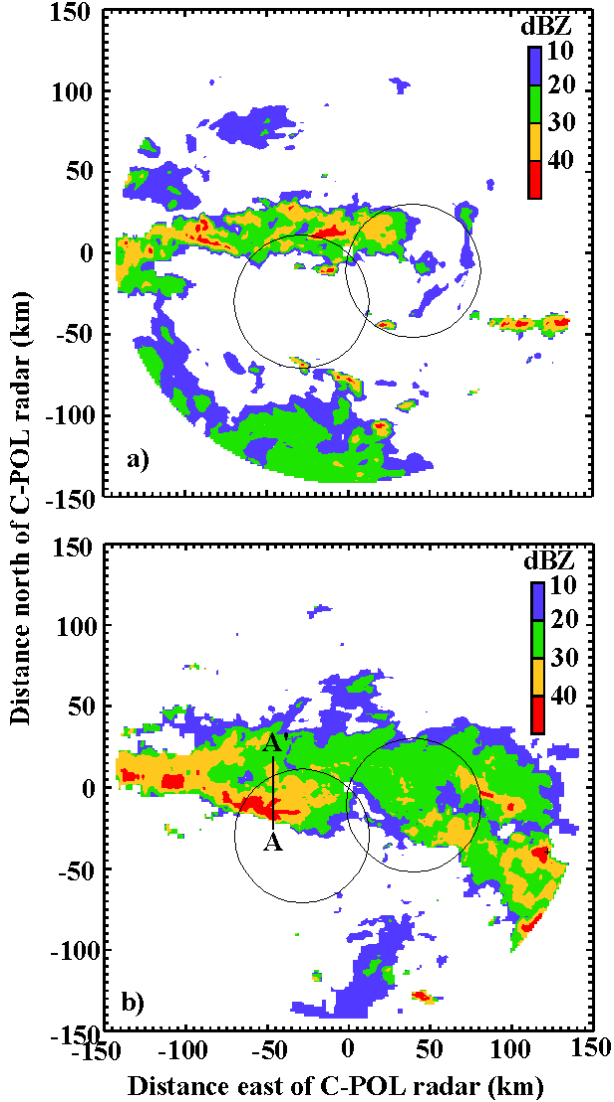


Figure 4 CPOL radar reflectivity (dBZ) at 2.5 km MSL at (a) 0430 UTC, and (b) 0800 LST, 20 May 1998.

The frontal precipitation system moved into the SCSMEX radar observation domain in the early hours of 20 May. At 0430 LST, the dominant feature was an east-west oriented rainband located to the north of the CPOL radar (Fig. 4a). The convection experienced a significant enhancement in intensity and areal coverage over the next six hours (Fig. 4b).

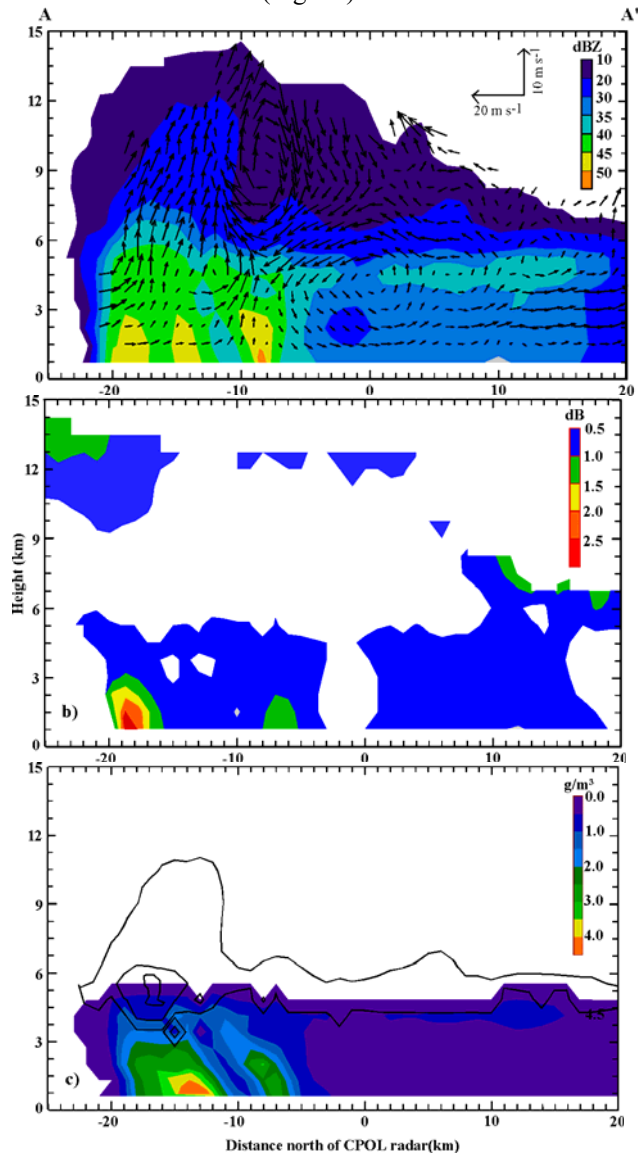


Figure 5 Vertical cross section along line AA' shown in Fig. 4 for a) radar reflectivity (shaded) and system-relative wind flow (vector), b) differential reflectivity (dB), and c) hydrometeor density: rainwater (g m^{-3}) (shaded) and ice water (contoured at 0.1, 0.5, 1.0 g m^{-3}) at 0800 LST 20 May 1998.

At 0800 LST, the convection was at its mature phase with the maximum radar reflectivity at about 55 DBZ and an echo top near 15 km MSL (Fig. 5a). There was a rapid reduction in reflectivity with height above the melting level (~ 4.5 km MSL) as a result of relatively weak updraft velocities in most tropical oceanic convection (Zipser and LeMone 1980). The airflow pattern contains some common characteristics of tropical oceanic convection. The low-level inflow was from the warm and moist tropical air ahead of the leading edge.

The center of the updraft was collocated with the convective core. There was a transition zone with weak radar reflectivity, generated by convective downward motion just behind the convective core. Following the transition zone, a stratiform rain echo, characterized by a radar reflectivity “bright band” (35–40 dBZ) near the melting layer, was located in the rear portion of the system. However, differences from the tropical convection documented for other regions, e.g. the western Pacific (Jorgensen et al. 1997), and the Atlantic (Houze 1977) are also noted. Usually, as a result of the convergence between incoming low-level flow and the outflow caused by the convection produced cold pool, the updraft zone is limited to a narrow ribbon-shaped area near the leading edge. However, the updraft of this system was in a wider region with a maxima extending to the rear part of the convective core.

The differential reflectivity (Z_{DR}) reached about 2.9 dB at the lowest levels close to the leading edge of the convection (Fig. 5b). That corresponded to drops of about 2.7 mm in diameter. However, the contour of 1 dB had a very small area coverage and was limited to below 3 km, well below the 0°C level. This indicated that oblate drops with diameter over 1.5 mm immediately fell out and were not lofted into the mixed phase region because of relatively weak updrafts at low levels. The mid-sized raindrops indicated by Z_{DR} of 0.5–1.0 dB in the convective part reached the level of 5.5–6 km. When the mid-sized drops were lofted to mid-levels, they followed the updraft track and then were slowly sorted out by size toward the rear of the convection. Elevated Z_{DR} (>0.5 dB) collocated with low Z_H (<30 dBZ) at heights of 6 km and higher in the trailing anvil region were likely associated with horizontally oriented ice crystals or aggregates of ice crystals. Meanwhile, the intense cell (Fig. 5c) exhibited maximum water content of over 4 g m^{-3} at the lowest 1.5 km level, collocated with the maximum reflectivity but behind the maximum Z_{DR} . This indicated that it was the small raindrops with D_m less than 1.5 mm at low-levels that contributed to the maximum rainwater content in the convective core. Given the weak updrafts at 3–5 km MSL, the lofting of raindrops above the freezing level in the developing convection was negligible. As a result, there is very little precipitation ice mass in the system.

b. Case of 24 May

The squall line system observed on 25 May 1998 includes three major lines persisting from 0400 to 2100 LST. Among them, the second squall line was the most intense one with the largest area coverage. At 1400 LST, the second squall line was at its mature stage showing a continuous convective band with the east-west extension up to 50 km (Fig. 6). The peak radar reflectivity of about 55 dBZ was recorded at 1.5–3.0 km MSL.

An important characteristic of this squall line was that the front to rear low-level inflow extended all the way to the very rear part of the cell. The deceleration of the low-level inflow from the front portion with the formation of a new cell behind the old cell was also evident. The low-level maximum updraft was also

located in the convection zone at the rear of the system. The strong updraft at the rear also implied that the inflow must pass a region ahead of the convective line before entering the convective tower. Downdrafts were located just ahead of the updrafts. Consistent with the weaker updrafts in a tropical oceanic environment, there was a sharp reflectivity gradient above the 0°C level.

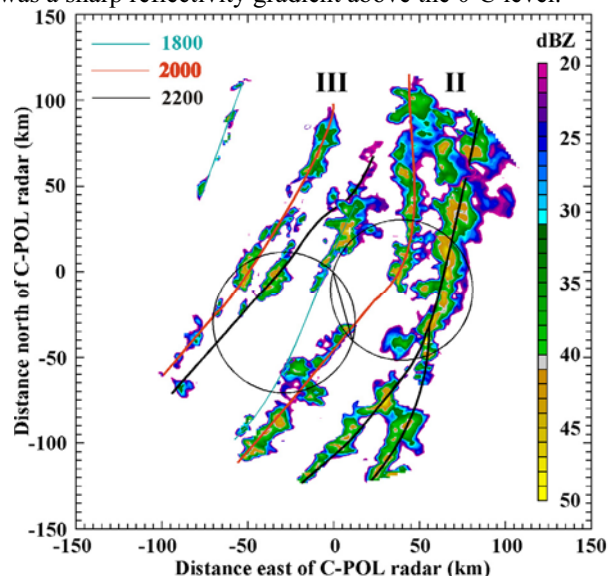


Figure 6 Time series of the CPOL radar reflectivity (dBZ) at 2.0 km MSL for the evolution of the main echoes of the second and third squall lines on 24 May.

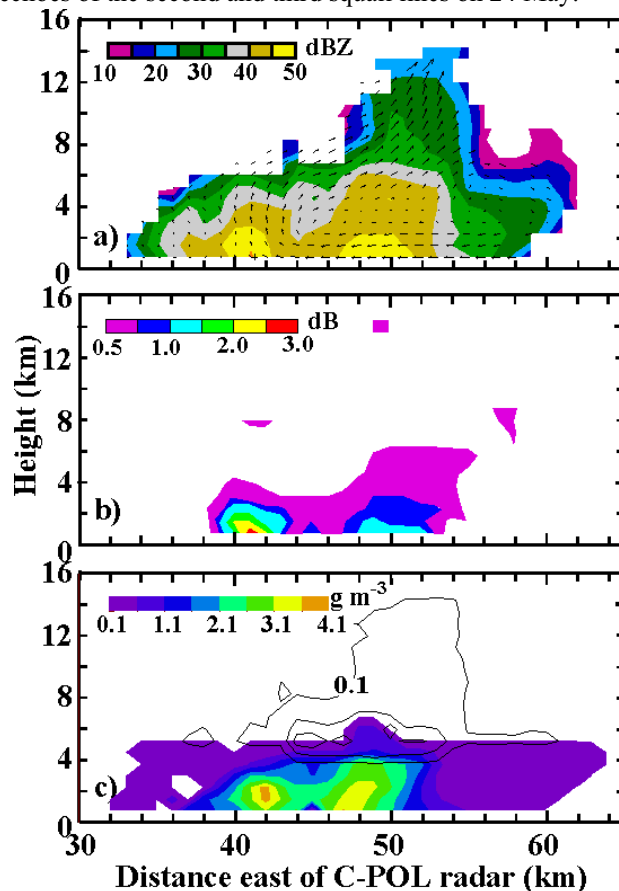


Figure 7 Same as Figure 5, but for variables retrieved at 1240 LST, May 24, 1998.

Similar to the case of 20 May 1998 discussed earlier, the Z_{DR} of 1 dB was also limited in the lowest 3 km, well below the 0°C level (Fig. 7b). Compared to other analysis of tropical MCS, e.g. in Maritime Continent by Carey and Rutledge (2000) and Amazon by Cifelli et al. (2002), the height and magnitude of the Z_{DR} column shown here were quite low. At the onset stage of the SCS summer monsoon, the low-level convergence and updrafts associated with the convection were relatively weak and not sufficient to lift hydrometers aloft to sub-freezing temperatures, e.g., to the level of mixed phase. For the case studied here, the low-level inflow had to pass a downdraft and cooled region before entering the updraft. Modified air in the low-level updraft may have reduced the buoyancy and hence updraft speed, contributing further to a low height and magnitude of the Z_{DR} column.

Cross-section of rainwater content exhibited comparable low-level (2 km) maxima in the developing (4 g m^{-3}) and mature (3.5 g m^{-3}) cells, at 41 and 49 km east of C-POL respectively (Fig. 7c). However, the kinematic and microphysical processes leading to these maxima at different stages of the convective lifecycle were somewhat distinct. In the developing cell, the maximum water content was located at 1.5-2.5 km above the maximum Z_{DR} . The gentle low-level updrafts allowed sufficient time for the collision-coalescence process to develop both large raindrops and high rainwater contents. However, the weak low-level updrafts were unable to lift the largest raindrops found at the lowest level further upward. Those large drops with mean D_m of 2.0-3.0 mm were offset below the maximum water content due to size sorting by the updraft. It was the drops of 1.5-2.0 mm at around 2 km that contributed to the maximum rainwater content in the developing core. Given the very weak updrafts at 3-5 km, there was no indication of the lofting of raindrops above the freezing level in the developing convection. As a result, there is very little precipitation ice mass in the developing cell. The lack of significant raindrop freezing also denied the extra buoyancy that is contributed by latent heat release of freezing to the growing cells.

In the mature cell, the low-level updrafts were still weak, promoting continued warm rain processes, but large raindrops ($D_m > 2 \text{ mm}$) had already precipitated out since the updrafts were unable to keep them aloft. As a result, the maximum rainwater content up to 3.5 g m^{-3} was collocated with the maximum Z_{DR} (1.0-1.2 dB) at the lowest level. Mid-level updrafts were larger in the mature as compared to the developing convection and were capable of lofting a small zone of supercooled rain drops about 1 km above the freezing level. Freezing of the supercooled drops caused a slight enhancement in the precipitation ice mass (0.6 to 1.2 g m^{-3}) at mid-levels (5-6.5 km) in the mature cell. However, the vertical extent of the Z_{DR} column was modest and hence supercooled drops and enhanced precipitation ice mass associated with frozen drops were present only in the lowest (or warmest) portions of the mixed-phase zone. In brief, the convection observed during the onset of SCS

summer monsoon is similar to the maritime-like convection over the Amazon during the westerly wind regime and very unlike the vigorous tropical continental convection during the easterly regime of the Amazon and the tropical island convection, which were both characterized by strong and vertically extensive Z_{DR} columns and hail/frozen drop zones.

References

- Carey, L. D., and S. A. Rutledge, 2000: The relationship between precipitation and lightning in tropical island convection: A C-band polarimetric radar study. *Mon. Wea. Rev.*, **128**, 2687-2710.
- Cifelli, R., W. A. Peterson, L. D. Carey, and S. A. Rutledge, 2002: Radar observation of the kinematic, microphysical, and precipitation characteristics of two MCSs in TRMM-LBA. *J. Geophys. Res.*, **107**(D20), 8077, doi:10.1029/2000JD000264.
- Ding, Y., and Y. Liu, 2001: Onset and the evolution of the summer monsoon over the South China Sea during SCSMEX field experiment in 1998. *J. Meteorol. Soc. Japan*, **79**, 255-276.
- Houze, R. A., Jr., 1977: Structure and dynamics of a tropical squall-line system. *Mon. Wea. Rev.*, **105**, 1540-1567.
- Jorgensen, D. P., M. A. LeMone, and S. B. Trier, 1997: Structure and evolution of the 22 February 1993 TOGA COARE squall line: aircraft observations of precipitation, circulation, and surface energy fluxes. *J. Atmos. Sci.*, **54**, 1961-1985.
- Lau, K.-M. et al, 2000: Report of the field operations and early results of the South China Sea Monsoon Experiment (SCSMEX). *Bull. Amer. Meteor. Soc.*, **81**, 1261-1270.
- Mohr, C. G., L. J. Miller, R. L. Vaughan, and H. W. Frank, 1986: The merger of mesoscale datasets into a common Cartesian format for efficient and systematic analyses. *J. Atmos. Oceanic. Technol.*, **3**, 143-161.
- Rutledge, S. A., E. R. Williams, and T. D. Keenan, 1992: The Down Under Doppler and Electricity Experiment (DUNDEE): Overview and preliminary results. *Bull. Amer. Meteor. Soc.*, **73**, 3-16.
- Tao, S. and Chen L., 1987: A review of recent research on the East Asian summer monsoon in China. *Monsoon Meteorology*, **60-92**. Chang, C.-P. and T.N. Krishnamurti, Eds., Oxford University Press, 353 pp.
- Wang, J.-J., 2004: Evolution and structure of the mesoscale convection and its environment: A case study during the early onset of south east Asian summer monsoon. *Mon. Wea. Rev.*, **132**, 1104-1120.
- Wang, J.-J. and L. Carey, 2005: Structure and evolution of an oceanic squall line during South China Sea Monsoon Experiment. *Mon. Wea. Rev.*, **133**, 1544-1561.
- Wang, J.-J., X. F. Li, and L. Carey, 2007: Evolution, structure, cloud microphysical and surface rainfall processes of monsoon convection during the South China Sea Monsoon Experiment. *J. Atmos. Sci.*, **64**, 360-380.

Zipser, E. J., and M. A. LeMone, 1980: Cumulonimbus vertical velocity events in GATE. Part II: Synthesis and core structure. *J. Atmos. Sci.*, **37**, 2458-2469.